Soft Spherical Tensegrity Robot Design Using Rod-Centered Actuation and Control

Lee-Huang Chen
Mechanical Engineering,
University of California, Berkeley,
Berkeley, CA 94720
e-mail: leehuanc@berkeley.edu

Kyunam Kim
Mechanical Engineering,
University of California, Berkeley,
Berkeley, CA 94720

Ellande Tang
Mechanical Engineering,
University of California, Berkeley,
Berkeley, CA 94720

Kevin Li
Mechanical Engineering,
University of California, Berkeley,
Berkeley, CA 94720

Richard House
Mechanical Engineering,
University of California, Berkeley,
Berkeley, CA 94720

Edward Liu Zhu
Mechanical Engineering,
University of California, Berkeley,
Berkeley, CA 94720

Kimberley Fountain
Mechanical Engineering,
University of California, Berkeley,
Berkeley, CA 94720

Alice M. Agogino
Mechanical Engineering,
University of California, Berkeley,
Berkeley, CA 94720

Adrian Agogino
Intelligent Systems Division,
NASA Ames Research Center,
Mountain View, CA 94035

Vytas Sunspiral
Stinger Ghaffarian Technologies,
Intelligent Systems Division,
NASA Ames Research Center,
Mountain View, CA 94035

Erik Jung
Computer Engineering,
University of California, Santa Cruz,
Santa Cruz, CA 95064

This paper presents the design, analysis, and testing of a fully actuated modular spherical tensegrity robot for co-robotic and space exploration applications. Robots built from tensegrity structures (composed of pure tensile and compression elements) have many potential benefits including high robustness through redundancy, many degrees-of-freedom in movement and flexible design. However, to take full advantage of these properties, a significant fraction of the tensile elements should be active, leading to a potential increase in complexity, messy cable, and power routing systems and increased design difficulty. Here, we describe an elegant solution to a fully actuated tensegrity robot: The TT-3 (version 3) tensegrity robot, developed at UC Berkeley, in collaboration with NASA Ames, is a lightweight, low cost, modular, and rapidly prototyped spherical tensegrity robot. This robot is based on a ball-shaped six-bar tensegrity structure and features a unique modular rod-centered distributed actuation and control architecture. This paper presents the novel mechanism design, architecture, and simulations of TT-3, an untethered, fully actuated cable-driven six-bar spherical tensegrity robot. Furthermore, this paper discusses the controls and preliminary testing performed to observe the system's behavior and performance and is evaluated against previous models of tensegrity robots developed at UC Berkeley and elsewhere. [DOI: 10.1115/1.4036014]

Introduction

Buckminster Fuller coined the term "tensegrity" in 1962 as a portmanteau of "tensile integrity" [1]. Tensegrity structures consist primarily of compression elements (rods) and tension elements (cables). The rods/cables of the structure experience pure compression/tension under equilibrium conditions. Tensegrity structures do not experience bending moments, which gives them the unique and beneficial characteristics of simplifying the design process and reducing the number of failure modes. The rods and cables are only required to withstand single axis loading [2].

Tensegrity structures exhibit the compliant behavior from their ability to distribute external forces globally. With this compliant characteristic, tensegrities can be used as a platform for soft robotic designs. Tensegrity soft robots have the ability to ensure that they will not injure humans during co-robotic applications, a critical trait behind the increased popularity in soft robots.

Tensegrity structures are of interest in the field of soft robotics due to their flexible and robust nature. They have the ability to passively distribute forces globally providing shock protection from unexpected impact forces. This feature makes them a robust mobile platform suitable for uneven and unpredictable environments in which traditional robots struggle.

The unique properties of tensegrity robots make them well-suited for a new generation of robotic landers/rovers for space exploration. The ability to land an inexpensive rover without damage and traverse uncertain territory is highly desirable for successful space exploration. In addition, the robot's intrinsic structural robustness allows it to handle or recover from unexpected and undesirable interactions with the environment (e.g., collision with obstacles) while moving. This could allow significantly faster scientific return as compared to current rover concepts that must meticulously plan every operation to provide adequate safety.

The UC Berkeley Emergent Space Tensegrities Laboratory has been collaborating with the NASA Ames Research Center on using tensegrity structures as the basis for next generation space exploration systems. Traditionally, rigid wheeled robots, like the Mars Curiosity rover, have been the primary space exploration platform. Heavy rigid robots require detailed sensing during

operation, while robust compliant robots like TT-3 can operate with minimal sensing at a fraction of the weight.

Prior Research

Prior work with tensegrity structures has focused on robust static structures in modern architectural, artistic, and structural applications. Examples include Snelson's unique, stable biotensegrity art pieces [3], Tibert's deployable tensegrity space structures [4], and Fu's large-scale tensegrity dome designs [5]. However, only recently, in parallel with the rise of soft robotics, tensegrities have come to the forefront of robotic design.

In examining examples of work on active tensegrity structures, the number of examples grows fewer. Of note are NASA Ames Research Center's work on the Spherical Underactuated Planetary Exploration Robot ball (SUPERball) and its predecessor, the Reservoir Compliant Tensegrity Robot (ReCTeR) [6,7]. Both SUPERball and ReCTeR are untethered, spherical tensegrity robots capable of cable-actuated deformation and motion. Unlike our TT-3 robot, both SUPERball and ReCTeR are under-actuated systems with 12 and 6 actuators, respectively.

The main advantages of the fully actuated (24 actuators) TT-3 tensegrity structure are (1) low-energy shape changes, (2) many degrees-of-freedom to change shape (could be useful for getting unstuck or positioning instruments), and (3) complete control of tension in the structure (could be useful for different tensions for packing, landing, and mobility).

The predecessor to the TT-3 (version 3) robot is the TT-2 (version 2) robot shown in Fig. 1, which is UC Berkeley's spherical tensegrity robot, featuring a similar six-bar tensegrity structure with 24 actuators. The six rigid members were constructed from balsa wood on the TT-1 (version 1) robot, eventually being upgraded to fiberglass struts on the TT-2 robot, while the tensional members were comprised of linear actuators in series with elastic cords [8]. Simulation work in NASA's Tensegrity Robotics Toolkit (NTRT) environment allowed for the development of multi-actuator strategies to efficiently generate punctuated, or stepwise, rolling motion.

Apart from spherical tensegrity robots, spinelike tensegrity structures have also been explored as a locomotion strategy with work being done on cable-connected and cable-actuated spine vertebrae as well as duct exploring robots with two tetrahedral frames linked by hinge joints and controlled with linear actuators [9–12]. EPFL's IMAC Laboratory has expandable tensegrities for dynamic use in rescue situations [13]. Paul et al. have demonstrated gait production in a three-strut, nine-cable arrangement [14,15].

The dynamic, highly specialized, and nonstandardized nature of tensegrity robotics has motivated the development of a rapid prototyping tensegrity system at UC Berkeley, in collaboration with NASA Ames. The development of TT-3 will help construct a modular hardware and controls framework for tensegrity-based robotic structures that will accelerate the research in this emerging field.
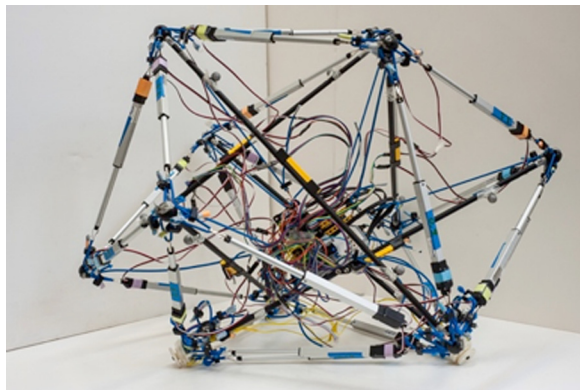

Fig. 1   TT-2 tensegrity robot with linear actuators

Rod-Centered Design

The original NASA target mission was the development of a lander/rover system that could explore Titan, the largest moon of Saturn. Some of the main design challenges are (1) a robot system that can sustain high-speed impact, (2) maneuver around the surface of the planet after landing, (3) carry a scientific payload, (4) transfer or absorb unexpected forces, and (5) be a low-cost, lightweight system. With these abilities, possible missions were expanded to include exploring the craters of Earth's moon.

With these target goals, tensegrity structures are predicted to be a good basis for a design platform as they have (1) the ability to distribute external forces globally, (2) a high strength to weight ratio, and (3) adjustable structure stiffness. The ability to distribute external forces throughout the structure means that the structure has the potential to absorb large impact forces from different forms of landing phases in the mission. The characteristic of the high strength to weight ratio provides the possibility of developing a lightweight system. Combining this ability to distribute forces globally with stiffness adjustments, it is possible for the structure to change its shape by changing the tension levels at different segments of the structure. With the proper control of this "shape-shifting" characteristic, the structure can perform punctuated rolling, which will be discussed in more detail in the Control and Actuation Strategy and Locomotion Experiments sections.

The middle point of the rod is the furthest location from the surface of the six-bar tensegrity. It is the best location to protect the critical components during rolling and impact. Therefore, the placement of all the critical components (e.g., controllers and actuators) at the center of the rods can potentially improve the reliability and functionality of the system.

Simulation Modeling

For simulation, we use NASA's Tensegrity Robotics Toolkit (NTRT) [16,17], an open-source tensegrity-specific simulator built to run on top of the Bullet Physics Engine (version 2.82). The NTRT data structure represents rods and strings as a tree of substructures that can be rotated and moved. Strings are represented in a two-point linear model using Hooke's law forces with linear damping.

In simulation, the dynamics and kinematics of different designs can be explored, and inherent advantages and disadvantages of adjustments in parameters can be compared. The NTRT simulator has the ability to have rapid development structures in this physics-based environment. Since tensegrity structures have complex internal force distributions at different states, NTRT can be used as a tool to assist with designing tensegrity robots. With NTRT, a six-bar structure with the known parameters, such as rod length, rod diameter, rod mass, and spring constant, can be modeled and its behavior simulated. With the modeled tensegrity, different pretension values can be applied to graphically visualize the appearance of the tensegrity structure.

Figure 2 shows a model of TT-3 that is simulated with three different pretension values. With a small tension value, TT-3 appears to be flat on the ground. With increasing tension, the structure will gradually stand up to be more spherelike. NTRT can estimate the required tension force for modeled structures. In the case of TT-3, the initial modeling of TT-3 with close estimation of system parameters shows the minimum tension required for the structure to be spherelike was 17.5 N. Knowing the potential tension requirement can help the designer better select critical components needed for the robot. This feature can greatly improve the efficiency of the design process and reduce the need for constant trial-and-error with designing physical prototypes.

Impact Dynamics

The compliant tensegrity structure has the ability to absorb forces during impact. This ability is due to the transfer of the energy throughout the system. During impact, the structure will
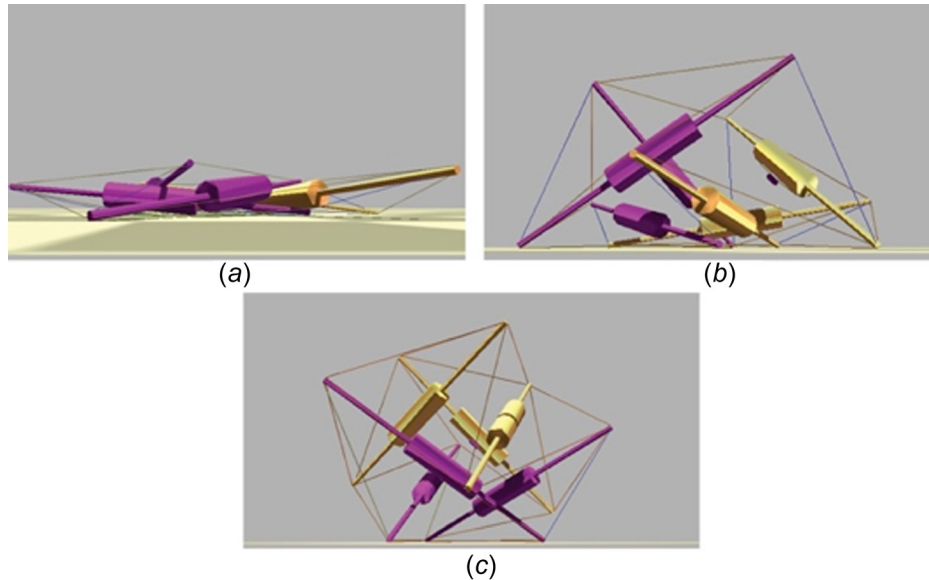
Fig. 2   NTRT simulations of TT-3 with increasing sequence (*a*)–(*c*) of different pretensions

deform; the deformation in the structure is the transfer of kinetic energy to the potential energy in the elastic element. For example, for a tensegrity structure using extension springs as its elastic elements, the springs will stretch to a higher potential state during impact. This is the transfer of the impact energy to strain energy in the springs. Therefore, it is potentially more valuable to have a structure that can be deformed more during impact.

In a tensegrity system, rods are the main components that contribute to the mass distribution and inertia of the system, and the contribution of cables is often neglected. As the rods do not touch each other and are only connected by the cables, each rod can be modeled as an individual subsystem of the structure subject to external forces such as the gravity and cable forces. As a result, the dynamic behavior of individual rods, which is affected by the rod mass distribution, collectively can be used as a simple model of the response of the overall structure. A different rod design will result in a different mass distribution across the rod, which in turn will affect the behavior of the rod upon impact. In order to see the differences, two simple cases are presented in Fig. 3. In the first rod design, the rod mass is concentrated at its center (Fig. 3(*a*)). Its mass moment of inertia with respect to the ground contact can be calculated with the following equation:

$$I_A = m \cdot \left(\frac{r}{2}\right)^2 = m \cdot \frac{r^2}{4} \qquad (1)$$

On the other hand, the second rod design divides the rod mass evenly on the two ends (Fig. 3(*b*)). In this case, the mass moment of inertia with respect to the ground contact can be calculated with the following equation:
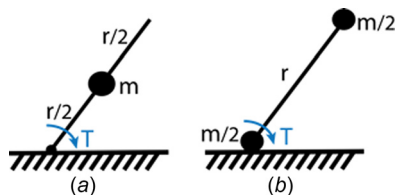
$$I_B = \frac{m}{2} \cdot r^2 \qquad (2)$$

If each rod is subjected to the same torque while the ground contact end is the pivot point, the different mass distribution will result in different angular acceleration as shown in Eq. (3)

$$T = I_A \cdot \alpha_A = I_B \cdot \alpha_B \qquad (3)$$

$$I_A = \frac{I_B}{2} \qquad (4)$$

$$\alpha_A = 2\alpha_B \qquad (5)$$

The result is that the rod in Fig. 3(*a*) will have twice the angular acceleration of the rod in Fig. 3(*b*) as shown in Eq. (5). The higher angular acceleration of the rod is one of the main benefits of the rod-centered design because it implies the structure will deform more when the same torque is applied. The larger deformation in the structure means the displacement of the springs or the elastic elements in the structure will be larger, increasing the shape shifting capabilities.

Impact Simulation

NTRT simulations [18] were performed on the fully modeled TT-3 system to confirm the difference in the behavior of the rods presented in Fig. 3 at the structural level during impact. From the Impact Dynamics section, the structure with mass at the center of the rod should be more compliant than the structure with its mass evenly divided at the two ends of the rod. This means that the former should deform more than the latter structure.

Figure 4 shows the sequence of both tensegrity structures with different mass distributions impacting the ground from the same height. All parameters of the two structures are the same except the location of the mass. The structure on the left in Fig. 4 has a large mass at the center of the rod, and the structure on the right has the same large mass but it is divided between the two ends of the rod. This simulation (Fig. 4) confirms the structure on the left is able to deform more during impact.

During the simulations, rod acceleration was recorded at the location where critical components are housed (the center capsule for TT-3 and the end modules used in previous prototypes). Data showing the initial impact in Fig. 5 illustrate the impact intensity experienced by critical components during landing. From the graph, it can be seen that the TT-3 architecture can better protect
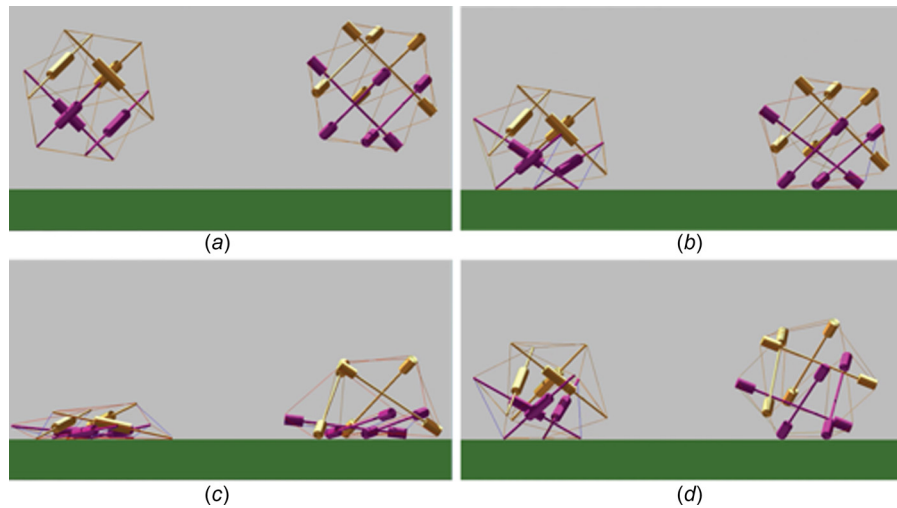

Fig. 3   A single rod of the tensegrity structure modeled: (*a*) with a mass at the center of the rod and (*b*) with two half masses on two ends of the rod. *T* is the applied torque, *m* is the rod mass, and *r* is the rod length.

Fig. 4 Sequence of impact from the same height of two tensegrity structures with different rod mass distributions

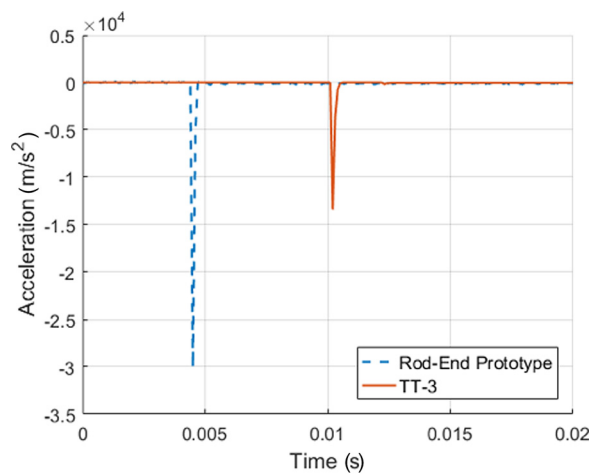**Fig. 5 Acceleration data of rod-centered TT-3 versus rod-end prototypes during impact in simulation**

Fig. 7 TT-3 deformation from different heights

the critical components as they do not come in direct contact with the ground and thus experience a lower magnitude of acceleration (high g forces) during impact.

Impact Experiment

To further study the impact absorption properties of the TT-3 robot, an adjustable drop test system was developed to consistently observe the robot during impact at various heights.
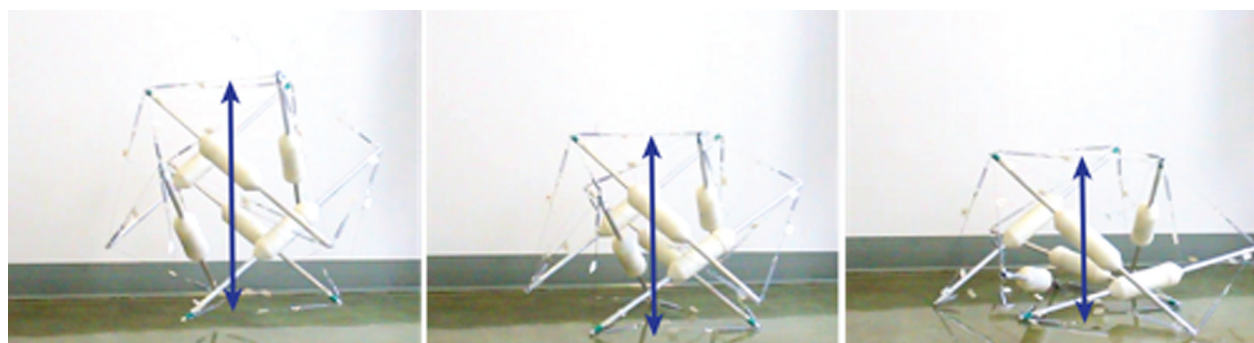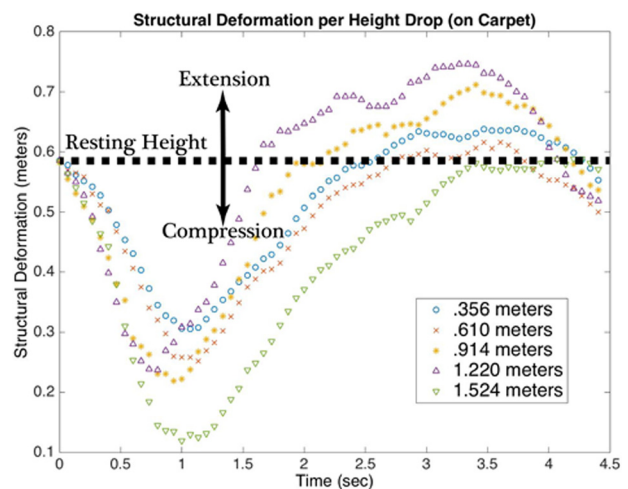
The TT-3 structure was dropped from five different heights. During each drop, a high-speed camera was used to record the deformation (top to bottom) from rest (25 in) of the tensegrity structures during impact (Fig. 6). Figure 7 is a plot of the deformation of the TT-3 structure from each height drop.

Hardware Design

The Impact Simulation and Impact Experiment sections have shown the benefits of locating the majority of the mass of the

Fig. 6 High speed video footage showing the deformation of the TT-3 structure during impact

system at the center of the rod. The goal of the research is to create a robot that can absorb the energy from landing and be actuated to perform locomotion. It is also important to design a robot that can maneuver around various terrains. It is shown in the Control and Actuation Strategy and Locomotion Experiments sections, that one mode of locomotion for tensegrity robots is to shift its center of mass outside of the base triangle to perform a punctuated roll.

An actuated cable in series with a spring is the chosen method for changing the shape of the structure to adjust the location of the projected center of mass. Cable actuation is chosen due to its ability to have long displacements between the nodes of the tensegrity robot. The range of displacement between the nodes of the structure can greatly determine the potential of shape shifting.

A simple motor and spool design is the selected method to change the length of cable between the nodes of the structure. This method allows for the ease of placement of the motor at a desired location, which is the center of the rod for TT-3.

Actuator Selection. After performing the required force simulation in NTRT, a few motors were selected as potential actuators for the robot. One key criterion during actuator selection was the high torque to weight ratio. The high torque to weight ratio creates the possibility to develop a lightweight tensegrity robot with a large range of tension adjustments and stiffness.

Three motors were selected: Pololu model 1595, Pololu model 2275, and Pololu 2218. They are all brushed DC motors because low cost is a goal for the overall system. The Pololu motor model 1595 weighs 10.5 g; the Pololu motor model 2275 weighs 103 g; and the Pololu motor model 2218 weighs 9.5 g. Both Pololu 2218 and 1595 are very lightweight, making them highly desirable as there will be 24 motors needed to construct a fully actuated robot.

Actuator Testing. The selected motors were tested with the EXTECH (EXTECH Instruments, Waltham, MA) heavy-duty digital torque meter to measure the stall. The motors were secured on a fixture, and voltage was supplied to the motors individually. The supply voltage was started at 1 V, and then increased with the increment of 1 V up to 9 V. At each voltage, the stall torque value was recorded. This process was used to observe the behavior of the motors at different voltages, and to compare with the manufacturer specification. Pololu 2218 was the chosen actuator through this process as the other two actuators did not perform reliably under high voltage.

Hardware Prototype

Actuation Module Using Acrylic Platform. The new design strategy was to design a modular actuation module that is located at the center of the rod. There are a total of 24 motors: six modules and four motors in each module. It is important to have a reliable and robust system for space exploration. Therefore, redundancy should be a key design feature. Consequently, TT-3 is designed with an individual microcontroller in each of its actuation modules.

Wireless communication is used as the main method for command signals and data transfer. The use of wireless units greatly simplifies the wiring, and no wires are required between the rods.

For the first prototype, an acrylic sheet was used as the platform for mounting all the components for the actuation module. Most of the components used were off-the-shelf, including a microcontroller, a wireless unit, a voltage regular, two motor drivers, four motors, and a battery pack. The hole patterns on the acrylic board were first modeled on a computer-aided design (CAD) program, then the pattern was exported to a laser cutter for manufacturing. Figure 8 shows the top and bottom of the assembled acrylic actuation module.

An enclosure was designed to house the actuation module. The enclosure has an internal rail for the acrylic plate to slide into with a cap placed over the open end to fully enclose the actuation module. Currently, the plastic enclosure shown in Fig. 9 is manufactured
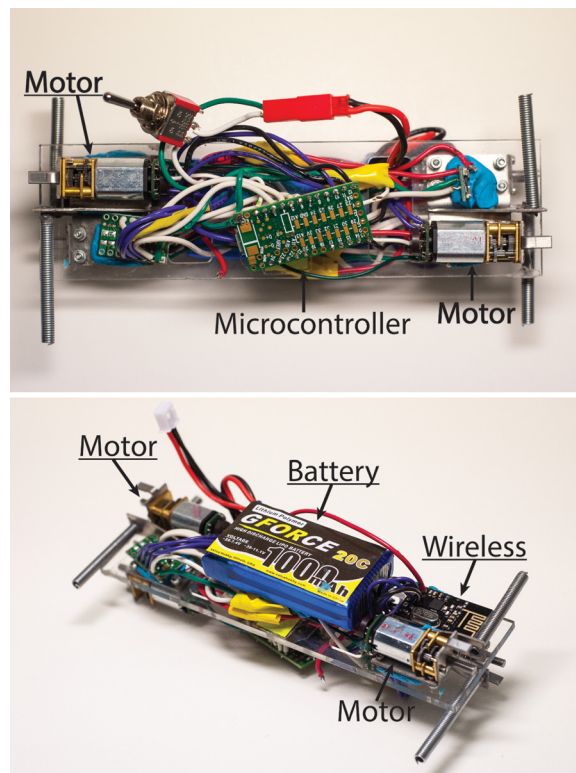

Fig. 8 Top and bottom of the actuation module with four motors, a microcontroller, a wireless unit, two motor drivers, a voltage regular, and a battery pack

with a fused deposition modeling (FDM) machine. Two 0.5 in diameter aluminum tubes are connected to both ends of the 3D-printed enclosure. One of the design features allows for the quick removal of the tubes, and the tube length can be adjusted for modularity. With different tube lengths, different sizes of tensegrity robots can be built, making the TT-3 platform modular and adjustable.

Actuation Module Using Printed Circuit Board (PCB). The acrylic plastic prototyped actuation module design described previously was able to provide promising results during preliminary testing. The TT-3 built with this actuation module was able to perform punctuated rolling with only a single motor actuated. However, the robot experienced unreliability during testing of long durations. Sometimes, the slave module would power off during rolling. After performing a failure mode analysis, it was discovered that the complex wiring on the actuation module was causing an inconsistent connection. In addition to the unreliability of the wire connections, the actuation modules were difficult to reproduce, which made it less ideal as a rapid prototyped robot.

The solution for this issue was the use of a custom printed circuit board as the replacement of the wires and acrylic support structure shown in Fig. 10. The custom printed circuit board (PCB) as the base structure for building the actuation modules not only increased reliability but also reduced the time and complexity
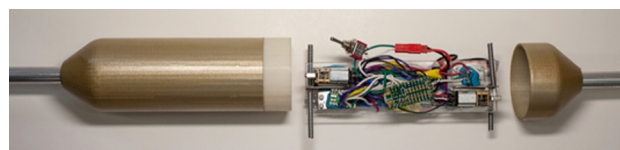

Fig. 9 Aluminum tubes, plastic enclosure, actuation module, and enclosure cap on each rod of the TT-3 robot. The actuation module slides into the plastic enclosure.
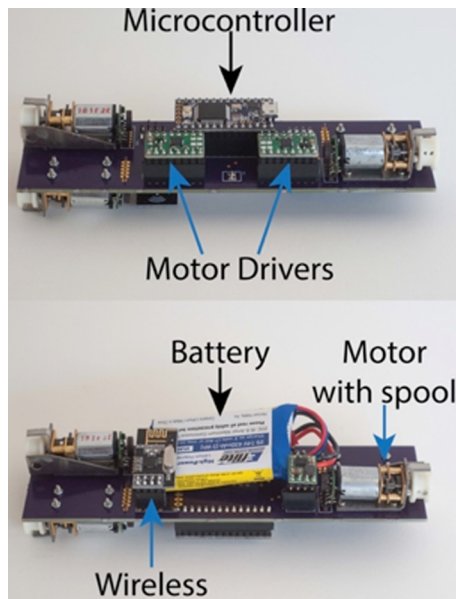
Fig. 10 This image displays the top and bottom of the actuation module using the printed circuit board as its base platform

of the prototyping process. The assembly time was reduced from 24 person-hours to eight person-hours for the full assembly of the six actuation modules.

Figure 11 shows how the printed circuit board actuation module is placed on TT-3, and how the cables are routed from the motors out to the neighboring rod to form the six bar tensegrity structure.

Endcap Design. Due to the relatively low power of the driving motors, any means of reducing cable friction in the robot will improve its functionality. For a cable-driven robot, the cables might experience high friction while in contact with material with different velocities or routings through corners. In the TT-3 system, one of the main locations of high friction force is the point of contact where the cable is routed out of the rod to connect with the neighboring rod. To address this issue, several endcaps were designed to fit on the end of the compression members in order to provide various routing methods for the cables. In addition to friction force reduction, these endcaps also need to provide nonpermanent connection points for the other two tension members that connect to the end of a compression member.

Direct Routing Through Polished Aluminum Tubes. The aluminum tubes have four holes drilled and polished on each end
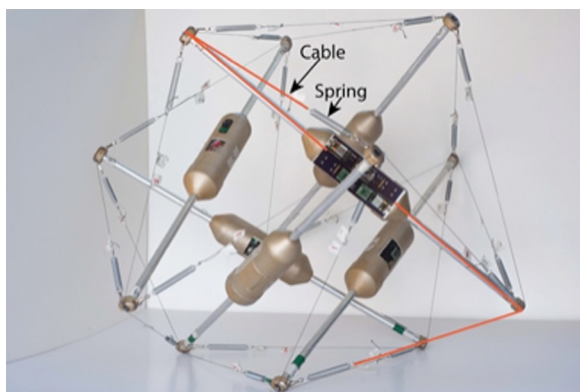
of the compression member. Two of the holes are used as the routing path for the cables inside of the rod to come out and connect to the neighboring rods. The two other holes are used to connect neighboring cables. Two types of end caps were investigated: 3D-printed acrylonitrile butadiene styrene (ABS) and polished aluminum.

Three-Dimensional-Printed ABS+ Plastic End Caps. One method for reducing friction is to guide the cables out of the hollow aluminum tubes that form the compression members by introducing a smooth contoured surface rather than having the cable travel over the edge of the tube. The first iteration was made of 3D-printed ABS+ plastic as shown in Fig. 12(a). Although it served its basic purpose, several flaws existed in the design. The cable still traveled over a relatively sharp angle while exiting the tube. Even though the design had an exterior fillet that reduced friction effectively, the ABS+ plastic was not resistant to wear which led to the cable wearing channels into the endcaps. These channels increased the cable wear, friction, and prevented the cables from sliding along the circumference of the tube during shape shifting. The off-the-shelf clips used as attachment points for the springs would also frequently tangle with the cables and were inconvenient to attach and detach from the endcap. Also, during punctuated rolling, wear was shown on the endcaps after hours of testing. Finally, with the elliptical outer geometry, the endcaps seemed to have an unpredictable behavior on dirt, sand and other types of rough terrain.

Machined Aluminum Endcap. A new set of aluminum endcaps were designed to address the shortcomings of the 3D-printed plastic endcaps. Machining the next design out of aluminum instead of 3D printing the design addressed the wear problems and reduced the friction by having the cables move on a polished machined surface instead of a rougher, 3D printed surface. The redesign could be prototyped quickly using standard machine shop tools to maintain the goal of a rapid prototyped robot. Due to the unreliability of the off-the-shelf clips for connecting and disconnecting the cables, an inset spring pin was designed as the new attachment system. However, the spring pins did not function as well as intended. They were meant to be inserted and removed by hand, but due to inconsistencies between pins as well as difficulty creating a hole of the required size for the desired fit, the attempted fits resulted in the pins being too difficult to insert or falling out when tension was released. In addition, a minor sharp edge from one of the milling operations was observed on all endcaps after detailed inspection.

To address the issue of minor sharp edges on the inner wall, the machining method and sequence was adjusted to produce a polished inner wall without defects from machining. In addition, the new design removed the spring pin system and replaced it with two easily machined vertical holes for tying a cable loop for attaching the springs shown in Fig. 12(b).
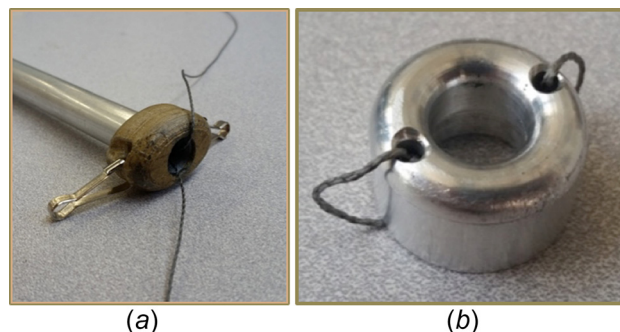

Fig. 11 TT-3, a six-bar spherical tensegrity robot with cables routed from the center module

(a)   (b)

Fig. 12 (a) Cable routed through 3D-printed endcap and (b) machined aluminum endcap

Endcap Evaluation. The endcaps were redesigned with the goal of lowering the friction force between the endcap and the cable. This friction delivers a large load on the motors causing them to stall if not handled properly.

An endcap testing platform was developed to quantify the static friction experienced on the cable from the endcap. This testing tool was able to repeatedly test various endcap designs to provide insights on the performance of the designs. With the endcap tester, the baseline performance for the current endcap was established and used to compare with future iterations.

The endcap was first installed on the tester shown in Fig. 13, then a cable was connected to both scales through the endcap and rod assembly. The turnbuckle was tightened until scale 1 read between 0.5 kg and 1 kg. The cable was pulled away from the endcap and toward scale 2 and then released. This was to ensure there was not a false binding force associated with tensioning the cable. After the readings on each scale were recorded, the turnbuckle was tightened to a higher tension force, and a new reading was recorded. This process was repeated until nine different tension readings were recorded. When the data collection was finished, the turnbuckle was loosened until the scales read again between 0.5 kg and 1 kg. The process was repeated until there were a total of four sets of data per endcap design.

As seen in Fig. 14, the data revealed an expected linear relationship between the reading on scale 1 and scale 2. The friction force between the cable and the endcap was determined by subtracting the two scale readings. A frictionless endcap would result in no difference between the two readings due to no external forces, so the ideal slope of the data would be 1 with a *y*-intercept of 0. Therefore, the slope of the line can determine the performance of different endcap designs regarding the friction force between the cable and endcap. The endcaps with high friction forces will have a line with low slope. With this information, the performance of different endcap designs can be ranked.

Figure 14 shows that the machined aluminum endcap had the least amount of friction between the cable and the endcap, followed by the 3D-printed ABS+ plastic endcaps. The cable routed through the aluminum rod without an endcap generated the most friction force.
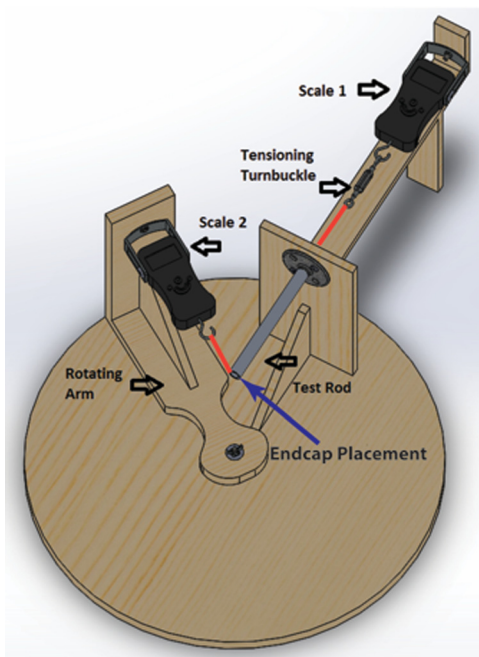
Control and Actuation Strategy

The TT-3 robot is based on a six-bar tensegrity structure, which is similar to an icosahedron, a spherical polyhedron. Unlike an icosahedron, the structure is missing six edges on its outer surface, resulting in a total of 24 cables, which form eight equilateral and twelve isosceles triangles. The most natural choice of locomotion for this robot is rolling based on its ball-shaped structure. However, the motion is discontinuous because the robot's outer surface is not perfectly smooth, and therefore, this motion is referred to as "punctuated rolling motion." The basic building block of this motion is a "step" which refers to a rotation of the body from one base triangle to another (Fig. 15). The TT-3 robot realizes this step by deforming its body shape by changing the lengths of its member cables in a shape-shifting manner. Not all deformations lead to a step; in order to make a successful step, the deformation should take the ground projection of the center of mass (GCoM) outside of the base triangle.

In a previous research, the authors developed actuation policies that resulted in the successful performance of punctuated rolling motion for a fully actuated and cable-driven six-bar tensegrity robot TT-2. The search method [18] and the multigeneration learning algorithm [8] were used to efficiently handle high dimensional control inputs. The symmetry of the structure was exploited when developing the actuation policies. The policies attempt to achieve two goals with the structure deformation: (a) reduce the area of the base triangle and (b) shift the position of GCoM as far as possible from the base triangle to make the structure unstable, thus leading to a step. Depending on the design of the tensegrity robot, multiple cables could be actuated simultaneously to make a step. For example, the TT-2 robot had a rigid linear actuator at the center of each cable edge, and this posed a limitation on the range of cable lengths that could be controlled [18]. As a result, the robot had a limitation on the maximum deformation it could achieve per cable actuation. For this reason, in order to achieve a step, at least three cables required actuation at the same time with the TT-2 robot.

The new design of the TT-3 robot can overcome this barrier. The edges of the TT-3 robot consist of cables and springs without any rigid body components; therefore, there is no mechanical restriction on how much a cable can be retracted, resulting in a greater deformation per actuation when compared to TT-2. In fact, a single cable actuation is sufficient to realize a step with the TT-3 robot. If one of the base triangle cables is fully retracted, the area of the base triangle becomes very small and the structure goes unstable. Hence, no additional actuation is required to shift the position of GCoM away from the base triangle because this will happen as a natural consequence of having a small area base
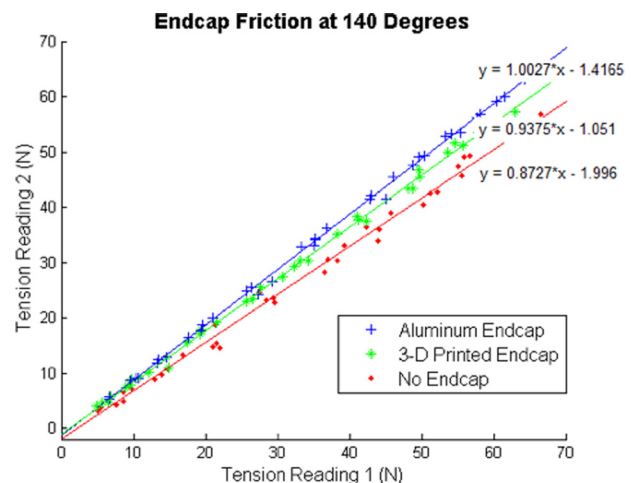

Fig. 13 Three-dimensional model of the endcap testing platform

Fig. 14 Plot displaying the relation of tension force on scale 1 and scale 2
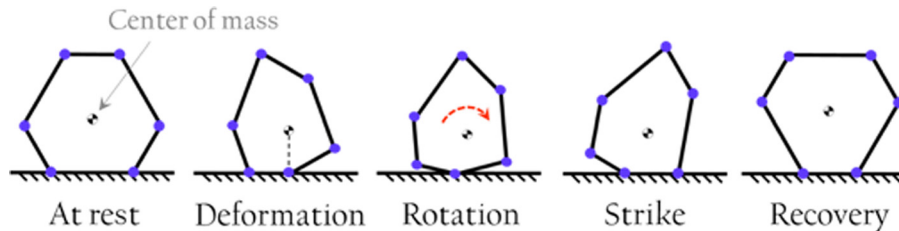
Fig. 15 A conceptual diagram that represents the different stages of shape-shifting performed by TT-3 to complete punctuated rolling

triangle. The direction of a step is determined by which edge of the base triangle is being actuated. There are a total of three edges in a triangle; therefore, at each face, there are three potential directions of travel shown in Fig. 16. In this work, only the single actuation strategy was implemented on the TT-3 as this was sufficient for the robot to move around on a flat ground. However, when moving on the uneven terrain (e.g., inclines), greater deformation may be favorable. In this case, the actuation policies developed in the authors' previous work [8,18] will be useful.

Currently, TT-3 uses wireless communication to signal the actuation commands. Each of the six actuation modules on the tensegrity robot has its own dedicated wireless communication unit. These wireless communication units act as slave units in the wireless network. The master wireless unit that is used to send commands to the slave unit is placed externally. However, there is

no difference between the master and slave units, and any of the slave units can serve as a master, untethering the communication system from external devices. The current communication architecture is chosen for ease of debugging.

With the current control, the desired motor encoder value is sent from the master module to the slave modules. The motor in the slave module will actuate the motor to the desired encoder count, and then send back the updated encoder value when the target is achieved. All 24 motors on TT-3 can be controlled through the method described above.
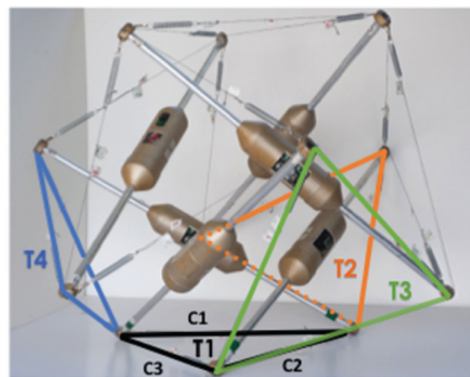
Locomotion Experiments

Various locomotion experiments were performed to observe the behavior of the TT-3 robot. The first test for the robot was to roll in a circular trajectory. The robot was able to successfully roll in a circular pattern continuously on the flat ground. The robot only required four steps to complete a full circle, and was able to roll continuously with a single actuation module.
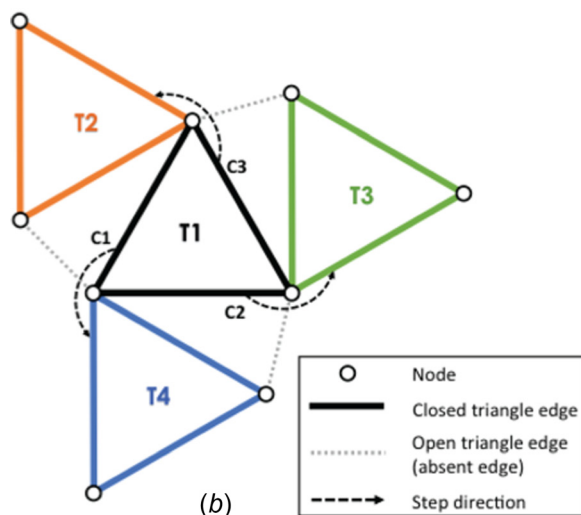
The second test was to walk in a forward trajectory. The robot was able to accomplish the forward motion through a zig-zag punctuated rolling style on a flat concrete floor with a measured forward motion velocity of 5 cm/s.

The third experiment with the robot was to perform forward punctuated rolling while carrying a simulated payload at the center of the robot. As shown in Fig. 17 with TT-3, this experiment helps visualize the interaction between the payload and the robot during locomotion. The payload did not interfere with the shape shifting required for a step during the experiment.

In addition to the indoor tests, TT-3 was tested to roll on the uneven outdoor terrain (Fig. 18). Not surprisingly, it appeared to be more difficult for the robot to roll on loose dirt than on a flat concrete floor. The rods of the robot seem to have dug into or dragged along the dirt during punctuated rolling. However, the robot was successful in performing the straight line roll command.

Conclusion and Future Research

TT-3, a six-bar tensegrity robot, has been demonstrated in this paper to be an effective mobile robot that can sustain impact. The robot was able to continuously roll in a circle with a single active actuation module and in a forward motion trajectory with three active actuation modules, with and without a payload at the center. A comparison of performance parameters of TT-3 with the rod-centered cable-driven design versus the previous TT-2 with linear actuators is provided in Table 1.

For space missions, we envision this payload containing sensors, spectrometers, cameras, or other light-weight scientific equipment. Based on its compliant nature, there are other potential co-robotic applications for TT-3. For instance, TT-3 can be envisioned as a medicine transport robot in a hospital environment. Due to its intrinsic compliance, the robot will not injure humans, which is one of its most important features.

Furthermore, the rod-centered design has shown to improve the system's ability to absorb impact and minimize damage to critical components like actuators and controllers. Although it has been shown that the TT-3 robot can absorb and dissipate energy during impact by greatly deforming its shape, the collision of the rods

(a)

(b)

Fig. 16 (a) A diagram of TT-3 with labeled based triangle T1 and three other neighbor triangles T2, T3, and T4. (b) The diagram displays the three cables C1, C2, C3 and its resulting triangle if actuated [8,10].

Fig. 17 TT-3 performs straight line walk while carrying a center payload

Fig. 18 TT-3 performs straight line walk on an uneven outdoor terrain

Table 1 Comparison of TT-2 and TT-3 tensegrity robots

	Rod length (m)	Weight (kg)	Maximum cable displacement (cm)	Speed (cm/s)
TT-2	0.69	2.7	10	1
TT-3	0.65	2	20	5

with each other during deformation has not been explicitly tested. Based on the preliminary physical hardware testing, it was shown that the TT-3 robot was not damaged by rod collision, but more elaborate analyses and experiments should be performed in order to guarantee the robustness of the robot under high g-forces [19]. In the future, impact tests with systematically changing physical parameters (e.g., pretension) to characterize the behavior of the robot under different impact conditions will be performed. Such tests will allow for optimization of the robot's design parameters to best survive significant impacts.

A current challenge with the robot is the lack of feedback control. The robot must be autonomous in order to successfully execute space missions where human supports are limited. This requires a high-level feedback controller as well as sensors to gather information about surroundings. The TT-3 robot does not have any functional sensors at this point, but we are in the process of integrating and testing different types of sensors such as inertial measurement units. Furthermore, a better performing control algorithm is under development that will allow the robot to move on the uneven terrain.

References

[1] Fuller, B., 1961, "Tensegrity," *Portfolio and Art News Annual*, Vol. 4, Art Foundation Press, Inc., New York, pp. 112–127.

[2] Skelton, R., Adhikari, R., Pinaud, J., Chan, W., and Helton, J. W., 2001, "An Introduction to the Mechanics of Tensegrity Structures," 40th IEEE Conference on Decision and Control (CDC), Orlando, FL, Dec. 4–7, pp. 4254–4259.

[3] Snelson, K., 2013, "Kenneth Snelson, Art and Ideas," Kenneth Snelson, Marlborough Gallery, NY, accessed Feb. 10, 2016, http://kennethsnelson.net/Kenneth Snelson_Art_And_Ideas.pdf

[4] Tibert, G., 2002, "Deployable Tensegrity Structures for Space Applications," Doctoral thesis, Department of Mechanics, Royal Institute of Technology, Stockholm, Sweden.

[5] Feng, F., 2005, "Structural Behavior of Design Methods of Tensegrity Domes," J. Constr. Steel Res., **61**(1), pp. 22–35.

[6] Sabelhaus, A. P., Bruce, J., Caluwaerts, K., Manovi, P., Firoozi, R. F., Dobi, S., Agogino, A. M., and SunSpiral, V., 2015, "System Design and Locomotion of SUPERball, an Untethered Tensegrity Robot," IEEE International Conference on Robotics and Automation (ICRA), Seattle, WA, May 26–30, pp. 2867–2873.

[7] Caluwaerts, K., Despraz, J., Iscen, A., Sabelhaus, A. P., Bruce, J., Schrauwen, B., and SunSpiral, V., 2014, "Design and Control of Compliant Tensegrity Robots Through Simulation and Hardware Validation," J. R. Soc. Interface, **11**(98).

[8] Kim, K., Agogino, A. K., Toghyan, A., Moon, D., Taneja, L., and Agogino, A. M., 2015, "Robust Learning of Tensegrity Robot Control for Locomotion Through Form-Finding," IEEE/RSJ International Conference on Intelligent Robots and Systems (IROS), Hamburg, Germany, Sept. 28–Oct. 2, pp. 5824–5831.

[9] Friesen, J., Pogue, A., Bewley, T., Oliveira, M. D., Skelton, R., and SunSpiral, V., 2015, "DuCTT: A Tensegrity Robot for Exploring Duct Systems," IEEE International Conference on Robotics and Automation (ICRA), Hong Kong, China, May 31–June 7, pp. 4222–4228.

[10] Mirletz, B., Park, I., Flemons, T., Agogino, A. K., Quinn, R. D., and SunSpiral, V., 2014, "Design and Control of Modular Spine-Like Tensegrity Structures," The 6th World Conference of the International Association for Structural Control and Monitoring (IACSM), Barcelona, Spain, July 15–17, pp. 5–10.

[11] Sabelhaus, A. P., Ji, H., Hylton, P., Madaan, Y., Agogino, A. M., Friesen, J., and SunSpiral, V., 2015, "Mechanism Design and Simulation of the ULTRA Spine: A Tensegrity Robot," ASME Paper No. DETC2015-47583.

[12] Friesen, J., Fanton, M., Glick, P., Manovi, P., Xydes, A., Bewley, T., and SunSpiral, V., 2016, "The Second Generation Prototype of a Duct Climbing Tensegrity Robot, DuCTTv2," IEEE International Conference on Robotics and Automation (ICRA), Stockholm, Sweden, May 16–21, pp. 2123–2128.

[13] Rhode-Barbarigos, L., 2012, "An Active Deployable Tensegrity Structure," Ph.D. dissertation, Department of Structural Engineering, Ecole Polytechnique Fédérale de Lausanne, Lausanne, Switzerland.

[14] Paul, C., Valero-Cuevas, F. J., and Lipson, H., 2006, "Design and Control of Tensegrity Robots for Locomotion," IEEE Trans. Rob., **22**(5), pp. 944–957.

[15] Paul, C., Robert, J. W., Valero-Cuevas, F. J., and Lipson, H., 2005, "Gait Production in a Tensegrity Based Robot," The 12th International Conference on Advanced Robotics (ICAR), Seattle, WA, July 18–20, pp. 216–222.

[16] NASA, 2014, "NASA Tensegrity Robotics Toolkit," National Aeronautics and Space Administration, Washington, DC, accessed June 15, 2015, http://ti.arc.nasa.gov/tech/asr/intelligent-robotics/tensegrity/NTRT/

[17] NTRT—NASA Tensegrity Robotics Toolkit, 2014, "TT-3 Simulation," National Aeronautics and Space Administration, accessed June 15, 2015, https://github.com/NASA-Tensegrity-Robotics-Toolkit/NTRTsim/tree/ArmModels/src/dev/eajung/v3Ball

[18] Kim, K., Agogino, A. K., Moon, D., Taneja, L., Toghyan, A., Dehghani, B., SunSpiral, V., and Agogino, A. M., 2014, "Rapid Prototyping Design and Control of Tensegrity Soft Robot for Locomotion," IEEE International Conference on Robotics and Biomimetics (ROBIO), Bali, Indonesia, Dec. 5–10, pp. 7–14.

[19] Berman, M. S., 2006, "Electronic Components for High-g Hardened Packaging," Army Research Laboratory, Report No. ARL-TR-3705.